International Journal of Applied Earth Observation and Geoinformation 23 (2013) 132–141

Contents lists available at SciVerse ScienceDirect

International Journal of Applied Earth Observation and Geoinformation

journal homepage: www.elsevier.com/locate/jag

Multitemporal fusion of Landsat/TM and ENVISAT/MERIS for crop monitoring

Julia Amorós-López[a,*], Luis Gómez-Chova[a], Luis Alonso[a], Luis Guanter[b], Raúl Zurita-Milla[c], José Moreno[a], Gustavo Camps-Valls[a]

[a] Image Processing Laboratory (IPL), Parc Científic, Universitat de València, 46980 Paterna, València, Spain
[b] Institute for Space Sciences, Freie Univertät Berlin, Carl-Heinrich-Becker-Weg 6-10, 12165 Berlin, Germany
[c] Faculty of Geo-Information Science and Earth Observation (ITC), University of Twente, 7500AE Enschede, The Netherlands

ARTICLE INFO

Article history:
Received 8 October 2012
Accepted 7 December 2012

Keywords:
Image fusion
Regularized spatial unmixing
Point-spread function
Multi-temporal NDVI
Crop monitoring

ABSTRACT

Monitoring Earth dynamics using current and future satellites is one of the most important objectives of the remote sensing community. The exploitation of image time series from sensors with different characteristics provides new opportunities to increase the knowledge about environmental changes and to support many operational applications. This paper presents an image fusion approach based on multiresolution and multisensor regularized *spatial* unmixing. The approach yields a composite image with the spatial resolution of the high spatial resolution image while retaining the spectral and temporal characteristics of the medium spatial resolution image. The approach is tested using images from Landsat/TM and ENVISAT/MERIS instruments, but is general enough to be applied to other sensor pairs. The potential of the proposed spatial unmixing approach is illustrated in an agricultural monitoring application where Landsat temporal profiles from images acquired over Albacete, Spain, in 2004 and 2009 are complemented with MERIS fused images. The resulting spatial resolution from Landsat allows monitoring small and medium size crops at the required scale while the fine spectral and temporal resolution from MERIS allow a more accurate determination of the crop type and phenology as well as capturing rapidly varying land-cover changes.

1. Introduction

Monitoring Earth's system dynamics using current and future Earth observation satellites enables a better understanding and characterization of the different phenomena and changes that occur on the Earth's surface at local and global scales. Remote sensing satellites provide support to many public administrations and private companies. For instance, mapping agencies require accurate up-to-date land-cover maps and change detection indicators to enable better understanding of remote sensing products and improved resource management, inventorying, and policy making. Therefore, from an operational perspective, there is an increasing need of data availability at high spatial resolution with temporal resolution shorter than one week. However, technological constraints impose a trade-off between spatial and spectral resolutions, and between spatial resolution and coverage, i.e., high spatial resolution usually implies low spectral and temporal resolutions and vice versa. Additionally, the impact of cloud cover reduces the operational use of image time series from satellites with low revisit time (8–16 days) and might hamper its use to monitor phenomena producing rapid variations in the surface. On the contrary, sensors such as MERIS (Rast et al., 1999) or MODIS acquire images of the same area every 1–3 days, but with coarser (and often insufficient) spatial resolution.

In this context, *image fusion* methods constitute a compelling field of research because they allow combining information from multiple sensors with different spatial, spectral, and temporal resolutions to obtain image products with improved overall characteristics (Stathaki, 2008; Pohl and Van Genderen, 1998). Remote sensing applications benefit from the use of image fusion in several ways: higher spatial and temporal coverage of the area of interest, along with improved reliability and system's robustness. For this reason, a wide variety of image fusion methods have been proposed in the remote sensing literature. Detailed reviews can be found in Pohl and Van Genderen (1998), Zhang (2004), Goshtasby and Nikolov (2007), Hall and Llinas (1997) and Thomas et al. (2008).

Image fusion is often used as a tool to increase the spatial resolution of satellite images by merging their radiometric (multispectral) data with the information from a high spatial resolution image. For instance, *pan-sharpening* methods (Wang et al., 2005; Alparone et al., 2007; Khan et al., 2009) are a particular case that makes use of a finer panchromatic (Pan) band in order to increase the spatial resolution of the multispectral bands. In this case, since both Pan and multispectral bands are commonly acquired by sensors mounted

* Corresponding author. Tel.: +34 963544061.
E-mail address: julia.amoros@uv.es (J. Amorós-López).

1569-8432/$ – see front matter © 2012 Elsevier B.V. All rights reserved.
http://dx.doi.org/10.1016/j.jag.2012.12.004

on the same platform, the same viewing geometry is preserved, which generally produces an accurate co-registration or matching among images. These pan-sharpening methods are commonly used for photo-interpretation applications so they usually give more priority to the injection of the spatial fine details in the multispectral bands in order to obtain a visually enhanced-RGB image (Aiazzi et al., 2011).

Multispectral and hyperspectral sensors provide valuable spectral information that must be preserved by the selected fusion method if the fused images are used for quantitative applications like studying vegetation dynamics or changes in reflectance over time. However, few image fusion methods yield reliable reflectance data. In the last years, data fusion approaches based on *spectral unmixing* have proven their value for delivering spectrally consistent fused images while reducing the mixed pixel problem (i.e., pixels composed of more than one land cover type) (Pellemans et al., 1993; Gao et al., 2006; Zurita-Milla et al., 2011). *Spectral unmixing* methods consider that a mixed pixel can be decomposed into a collection of pure spectra, or endmembers, and a set of fractional abundances that indicate the proportion of each endmember (Keshava and Mustard, 2002).

Mixed pixels from medium spatial resolution sensors, like MODIS (2 bands at 250 m, 5 bands at 500 m, and 29 bands at 1 km) or MERIS Full Resolution (FR) product (15 bands at 300 m), can be better described with the spatial distribution of land covers at the finer scale of Landsat (30 m). This assumption was used by the spatial and temporal adaptive reflectance fusion model (STARFM) (Gao et al., 2006) for combining information from the Landsat and MODIS sensors. Likewise, unmixing algorithms merging information from MERIS FR and Landsat images were used by Minghelli-Roman et al. (2001, 2006) and Zurita-Milla et al. (2008) to improve the spatial resolution of MERIS data. These methods, based on Zhukov et al. (1999), used a constrained *spatial unmixing* algorithm to increase the spatial resolution of the MERIS bands by using the spatial information provided by the Landsat image. This spatial information is typically obtained by applying unsupervised or supervised classification of the Landsat image into K classes so that mixed pixels can be characterized by their fractional composition. The main drawback of these approaches is the low spectral variability obtained for the K classes. To mitigate this, fusion is performed into a sliding window, which increases the class variability among windows. Nevertheless, the intra-class variability is discarded inside the window. In Amorós-López et al. (2011), this problem was addressed by using a soft clustering, which provides the land-cover class proportions for each pixel at Landsat resolution and is used to obtain mixed pixels in the fused image.

In this paper, we propose a multi-temporal setting of the algorithm that is applied to full MERIS and Landsat TM time series. The final goal is to complete or fill gaps in the Landsat time series by using MERIS data with more frequent coverage. Hence obtaining consistent time series at high spatial resolution. The potential of multitemporal land cover mapping and monitoring using MERIS data has been assessed by numerous studies at global (e.g. GlobCover product in Arino et al. (2007)) and national scales (e.g. Clevers et al. (2007), Dash et al. (2007) and Carrão et al. (2010)). However, better resolutions are frequently required to properly assess land cover changes in heterogeneous landscapes or for crop monitoring. The enhanced time series obtained using Landsat-like (20–30 m) and MERIS-like (250–500 m) images allow developing operational applications that require monitoring rapidly-varying phenomena and high spatial resolution, such as precision agriculture, irrigation advisory services, and near real-time change detection. Results show the validity of the processing scheme, both in terms of fusion quality assessment and consistency of the derived NDVI multitemporal products.

The remainder of this paper is organized as follows. In the next section, the downscaling approach is presented. Section 3 describes the study area and the image time series used in the experiments. In Section 4, the fusion approach is illustrated using Landsat/TM and ENVISAT/MERIS time series and a quantitative and qualitative assessment is also carried out. Finally, summary and conclusions of this work are given in Section 5.

2. Proposed methodology

The image fusion approach proposed in this work assumes a linear mixing model for the medium spatial resolution observations. Specifically, each MERIS pixel is unmixed using information about its composition, in terms of land-cover class proportions, which are obtained from the high spatial resolution images, i.e., the Landsat TM image time series. The proposed scheme is illustrated in Fig. 1, and the processing steps are summarized as follows:

1. First, a land-cover map at high spatial resolution is obtained performing a soft clustering on the Landsat image time series, and the membership of Landsat pixels to each cluster is calculated as posterior probabilities (Step 1).
2. Next, these posterior probabilities at the Landsat spatial resolution are used to get the abundance or class proportions for each MERIS pixel taking into account its actual point spread function and observation geometry (Step 2).
3. Then, a sliding-window *spatial unmixing* is carried out on the MERIS image. In this step, the proportions of the MERIS pixels within the window are used to obtain the endmembers of the classes through the inversion of a system of linear mixture equations (Step 3).
4. Finally, the fused pixels at high resolution are obtained as a linear combination of the estimated MERIS endmembers of each class weighted by the corresponding Landsat membership (Step 4).

These four steps will be explained in more detail in the following subsections.

2.1. Multitemporal clustering (Step 1)

The first step of the algorithm aims at obtaining an updated land-cover map with the highest spatial resolution available. For this purpose, one might use an existing land-cover map (Zurita-Milla et al., 2009) or alternatively generate a new one by classification

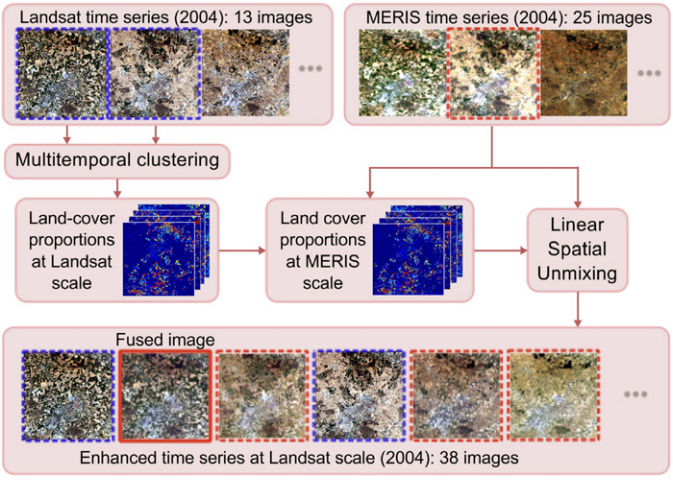

Fig. 1. Proposed multitemporal fusion scheme for the medium (MERIS) and high (Landsat TM) spatial resolution images.

of a high spatial resolution image (Zhukov et al., 1999; Minghelli-Roman et al., 2001; Zurita-Milla et al., 2008).

In the presented multitemporal setting, Landsat images in the time series are used to obtain the land-cover map. While one could stack all available images to obtain such classification map, we propose focusing only on the most close-in-time images to the date of the medium spatial resolution image in order to preserve the temporal consistency in the image fusion procedure. An unsupervised clustering is used to classify the Landsat TM image as in Zhukov et al. (1999), Minghelli-Roman et al. (2001), Zurita-Milla et al. (2008) but including the temporal dimension as well. We perform the multitemporal clustering by stacking the (6 + 6) spectral channels of the two Landsat image dates at 30 m as input features. This allows us to classify significant land cover changes between dates as a separate land cover class (cluster). Additionally, to stress the land cover changes, the Mahalanobis and the spectral angle mapper (SAM) distance maps obtained by comparing the Landsat spectra of both dates are also used as inputs of the clustering algorithm.

In this work, Landsat images are classified in K clusters using a self-organizing map (SOM) clustering (Kohonen, 2001). Nevertheless, other clustering algorithms may be equally used, such as k-means, Gaussian mixture models, or graph-cuts algorithms. Therefore, the method requires the definition of the number of clusters K to be found in the image, which depends on the area covered by the multispectral sensor. Heterogeneous landscapes typically require larger number of clusters. The optimal number can be determined from previous land-cover maps of the study area or by analyzing the impact on the final solution.

Classifying images by means of clustering algorithms usually provides a land-cover map where each pixel is assigned to a single class (hard or crisp clustering), which is typically done associating each input sample only with the nearest cluster center. However, the distances between each input and the clusters centers can be used to obtain a degree of membership to each cluster, which means that each input can belong to more than one class at the same time (soft or fuzzy clustering). This fact will be exploited in our algorithm as well.

Hereafter, superscript (M) refers to MERIS pixels and superscript (L) to Landsat pixels (or the finer spatial scale). The soft clustering approach yields a relative membership to each pixel in the clustering solution. We modeled this as a monotonic decreasing function (Alpaydin, 1998):

$$a_{ik}^{(L)} = \frac{(||\mathbf{s}_i^{(L)} - \boldsymbol{\mu}_k||_{\Sigma})^{-2/(m-1)}}{\sum_{k=1}^{K}(||\mathbf{s}_i^{(L)} - \boldsymbol{\mu}_k||_{\Sigma})^{-2/(m-1)}} \quad (1)$$

where $\mathbf{s}_i^{(L)}$ is the Landsat pixel i, $\boldsymbol{\mu}_k$ is the cluster centroid k, m is a *softness* parameter in the range $[1,\infty)$ (good results are typically obtained in [1.1,5]), and Σ is the sample covariance matrix implementing the Mahalanobis distance. In order to include the abundance sum-to-one constraint in the linear unmixing, the proposed abundances are normalized so that the membership of each pixel sum to one.

2.2. Land-cover fractions at MERIS scale (Step 2)

In the second step, the land-cover class proportions for each MERIS pixel are estimated from the proportions calculated in the Step 1. A perfect co-registration between the involved images is required to estimate the proportions from the same observed area. This co-registration can be done by mapping the images from the different sensors onto a common grid. However, this process, known as gridding, may introduce undesirable artifacts and misregistrations between observations (Gómez-Chova et al., 2011). For this reason, in this work, the MERIS image is not resampled to a common reference grid but each individual observation (pixel footprint) is projected onto the Landsat image to consider more precisely the actual common observed area. This pixel footprint is characterized taking into account the satellite's viewing geometry. Furthermore, the AMORGOS tool (ACRI-ST and ESA, 2007) is used to obtain a more accurate geolocation (longitude, latitude, altitude) for each MERIS pixel than those distributed in the MERIS L1b product.

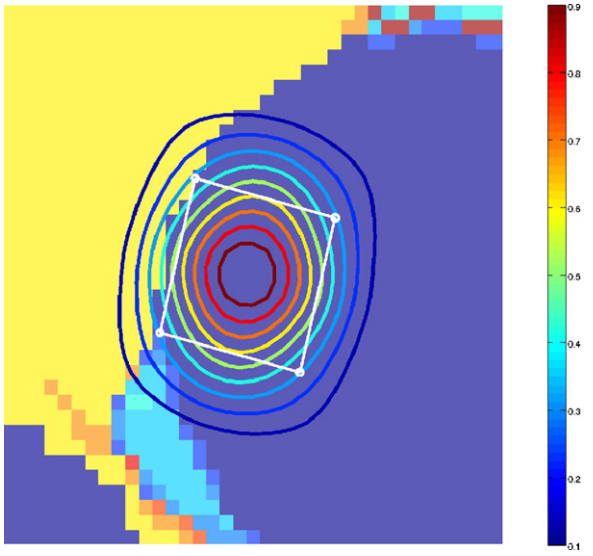

Fig. 2. Point spread function (contour lines) of a MERIS pixel projected over the land-cover map at Landsat scale taking into account the MERIS pixel footprint (white polygon).

The proportions of land-cover classes in a MERIS pixel j can be estimated as the average of the estimated class proportions of Landsat pixels within the MERIS pixel footprint $\mathcal{P}_j$:

$$a_{jk}^{(M)} = \frac{1}{|\mathcal{P}_j|}\sum_{i\in\mathcal{P}_j} a_{ik}^{(L)} \quad (2)$$

where $a_{ik}^{(L)}$ is the previously estimated contribution of class k in the Landsat pixel i and $|\mathcal{P}_j|$ is the number of Landsat pixels within the footprint of a MERIS pixel j.

These class proportions at MERIS scale can be further improved by considering the MERIS point spread function (PSF), which allows to properly weight the contribution of pixels from the high spatial resolution image to this particular MERIS observation. Including this information simply translates into a spatial convolution operation:

$$a_{jk}^{(M)} = \sum_i \mathrm{PSF}_{ji} a_{ik}^{(L)} \quad (3)$$

Note that a particular PSF is estimated for each MERIS pixel involved in the fusion procedure because it is obtained by projecting into the Landsat image the MERIS PSF adapted to the particular footprint (Fig. 2), which depends on the viewing observation geometry. A further analysis on the impact of the viewing geometry and the PSF effect on the solution is performed in Section 4.5.

2.3. Sliding-window spatial unmixing (Step 3)

In the third step, the MERIS image is processed in windows of size $w \times w$ centered in each pixel $s_j^{(M)}$. The central MERIS pixel is unmixed by using the contextual information of its neighboring

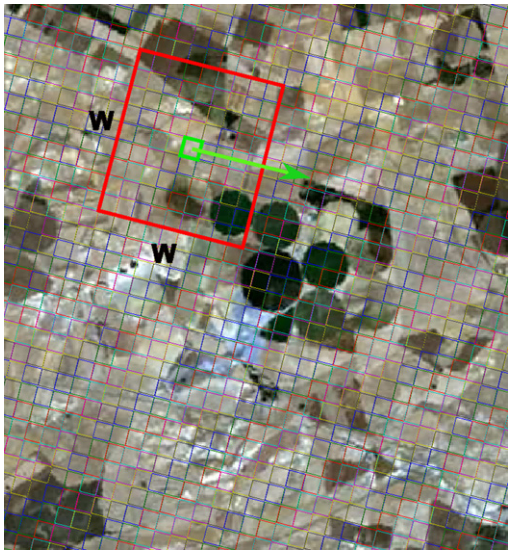

Fig. 3. Geometry of the sliding-window spatial unmixing. The central MERIS pixel (green polygon) is unmixed using the land-cover composition (provided by the Landsat image) of the the neighboring pixels within a window of size $w \times w$ (red polygon). (For interpretation of references to colour in this figure legend, the reader is referred to the web version of this article.)

pixels, as Fig. 3 illustrates. In each MERIS window, a linear spatial unmixing is performed by solving the linear equations system

$$\underbrace{\mathbf{S}^{(M)}}_{w^2\times N} = \underbrace{\mathbf{A}^{(M)}}_{w^2\times K}\underbrace{\hat{\mathbf{E}}^{(M)}}_{K\times N} + \underbrace{\boldsymbol{\varepsilon}}_{w^2\times N} \tag{4}$$

where $\mathbf{S}^{(M)}$ are the actual MERIS spectra in the window $\mathcal{W}$ of size $w \times w$, $\hat{\mathbf{E}}^{(M)}$ are the reference spectra to be estimated for each class in the window, K is the number of classes, N is the number of MERIS bands, and ε are the assumed errors or residuals of the linear model.

Note that, typically, a reduced number of classes will be present in each sliding-window so the abundances $a_{jk}^{(M)}$ often shrink to zero for some endmembers, i.e., the spatial unmixing in (4) will be solved using a reduced number of K classes in each window. In addition, in order to decrease residual errors in the estimation of MERIS endmembers, land-cover classes with proportions lower than 5% within a MERIS pixel ($a_{jk}^{(M)} < 0.05$) are discarded. It should be emphasized again that, unlike standard spectral unmixing, we are estimating endmembers instead of abundances.

This problem is solved individually for each MERIS spectral band by optimizing:

$$\hat{\mathbf{E}}^{(M)} = \min_{\hat{\mathbf{E}}} \left\{ \sum_{j\in W} \left[s_j^{(M)} - \sum_{k=1}^{K} a_{jk}^{(M)} \hat{e}_k^{(M)} \right]^2 \right\} \tag{5}$$

where the index of the spectral band has been intentionally omitted, i.e., this problem is solved as many times as MERIS channels until all the spectral bands of the endmembers $\hat{\mathbf{E}}^{(M)}$ are estimated. Note that the spatial unmixing process could be carried out for the whole image at once, but then only one pure spectrum per land-cover class would be found, hence disregarding the spectral variability. Besides, in this case, the number of classes needed for adequately characterizing the scene would increase significantly (Minghelli-Roman et al., 2006).

The sliding window approach allows us better capturing the variability for a given land cover at the cost of incorporating one more free parameter to study: the optimal window size. The window should contain enough MERIS pixels to allow a robust system inversion and permit a correct characterization of the pure spectra present in the MERIS pixel for the sake of good fusion quality. Besides, the size of the window should be small enough to reflect the intra-class variability of the high spatial resolution image (Landsat) to avoid the aforementioned spectral collapse, i.e., same endmember for a given land-cover class over the whole image.

2.3.1. Regularized linear unmixing

An additional problem appears from the band-by-band unmixing approach. The endmembers that minimize the quadratic error in the linear mixing model (5) are obtained independently for each spectral band. Hence, the spectral shape of these endmembers is not imposed in any way, which may produce unrealistic estimated spectra. Furthermore, spectral unmixing can be also affected by collinearity problems in which the high correlation between endmembers lead to inversion of ill-posed matrices. Hence, inversion model becomes unstable and the error term increases (Van der Meer and Jia, 2012).

In this paper, we alleviate these problems by including a regularization term in the cost function (Zhukov et al., 1999):

$$\hat{\mathbf{E}}^{(M)} = \min_{\hat{\mathbf{E}}} \left\{ \sum_{j\in W} \left[s_j^{(M)} - \sum_{k=1}^{K} a_{jk}^{(M)} \hat{e}_k^{(M)} \right]^2 + \alpha \frac{w^2}{K} \sum_{k=1}^{K} [\hat{e}_k^{(M)} - \bar{\mathbf{s}}_k^{\prime(M)}]^2 \right\} \tag{6}$$

where $\bar{\mathbf{s}}_k^{\prime(M)}$ is a *predefined* endmember *per* class, and α is a regularization parameter that precludes found endmembers in the window to differ too much from the imposed expected class spectra $\bar{\mathbf{s}}_k^{\prime(M)}$. Note that although this problem is also solved band-by-band, the range of possible spectral shapes is somehow controlled by the second term in (6) since the predefined endmembers are fixed.

The predefined endmembers are selected among the MERIS pixels yielding higher abundance levels for each class, and are selected directly from the image in order to have the same atmospheric conditions and spectral/radiometric biases. Alternatively, the predefined endmembers can be derived from the image using endmember extraction algorithms (Plaza et al., 2004, 2011; Camps-Valls et al., 2011).

2.4. Spectral assignment (Step 4)

In the last step, the estimated endmembers for the land-cover classes in each MERIS window $\mathcal{W}$ are used to reconstruct the central MERIS pixel in the window at the Landsat scale. Once the class endmembers for each window are estimated, one could simply assign to each Landsat pixel the corresponding endmember spectrum depending on the pixel's class label. This approach is suboptimal since all pixels of the same class in the analyzed window would have the same signature, thus no spectral variability would be captured. An alternative approach consists in using the posteriors from the Landsat soft clustering, $a_{ik}^{(L)}$, to generate the high spatial resolution fused pixels into the evaluated MERIS pixel

$$\hat{\mathbf{s}}_i^{(L)} = \sum_{k=1}^{K} a_{ik}^{(L)} \hat{\mathbf{e}}_k^{(M)} = \hat{\mathbf{E}}^{(M)} \mathbf{a}_i^{(L)}, \tag{7}$$

which can be expressed in matrix notation as $\hat{\mathbf{S}}_{fused}^{(L)} = \hat{\mathbf{E}}_W^{(M)} \mathbf{A}_P^{(L)T}$, where $\mathbf{A}_P^{(L)}$ contains class proportions for all Landsat pixels within the MERIS pixel footprint $\mathcal{P}$. Finally, an image product with the spatial resolution of Landsat (30 m) and the spectral resolution of MERIS (15 bands) is generated.

2.5. Final remarks

The spatial unmixing approach introducessome key improvements to increase the spectral variability of the land-cover classes in the fused products, which is the main drawback accounted in the literature for unmixing-based image fusion techniques (Park and Nab, 2007). The proposed soft clustering provides the land-cover class proportions at high spatial resolution that allows estimating the abundances at MERIS scale more adequately. These abundances are also used at the end of the process to obtain the pixels in the fused image as a realistic mixture. This guarantees the spectral variability of the land-cover classes inside the sliding-window and, by extension, in the fused product. We also characterize the MERIS PSF to combine the corresponding MERIS and Landsat observations and it is also used to weight more precisely the land-cover contributions at Landsat scale in the mixing process. Furthermore, a regularization term was added to the cost function to constrain the spectral shape of the endmembers, which also makes the solution more robust on both free parameters: the window size and the number of classes.

Finally, the proposed methodology could be applied to other Landsat-like and MERIS-like sensors, such as the future Sentinel 2 and 3 satellite series, respectively. These satellites will provide a new Earth observation framework where the availability of consistent time series will play an important role in many fields. The soft clustering would be calculated using the 1–10 bands from Sentinel-2/MSI and then the spatial unmixing would be performed using the 21 bands from the OLCI instrument on board Sentinel-3. In addition, the method can be directly applied to combine Landsat TM and MODIS sensors using the MODIS bands 1–7 at 250 m. However, the quality of the fused product might be affected by the actual resolution of this MODIS product, which bands 3–7 are upgraded from 500 m to 250 m. Hence, a further study will be required to assess the method's performance when combining Landsat and MODIS data.

3. Study area and image time series

Two time series of Landsat TM and MERIS Full Resolution (FR) images acquired over Albacete (Spain) in 2004 and 2009 are used to illustrate the capabilities of the multitemporal image fusion approach. The region covers an irrigated agricultural area (Barrax site), which is characterized by large and uniform land-use units. The main cultivated crops in the region are: cereals (barley, wheat, corn, and oat), potatoes, sugar beet, sunflower, alfalfa, and vegetables (onion, garlic, melon, and tomatoes). A urban area, Albacete city (39.0° N, −1.86° E), located at the bottom of the image is also included.

The selected study area (30×30 km) is located in the overlap area between adjacent Landsat orbits (reference grids 200-33 and 199-33) in order to get an additional acquisition between two nominal Landsat acquisitions (revisit time of 16 days). These additional images are very useful to better assess phenological changes and are also used as reference images for validation purposes.

In this work, cloud free images were manually selected from the two time series by visual inspection. These image series are composed of 13 Landsat and 25 MERIS images from April to December in 2004, and 11 Landsat and 39 MERIS images from February to December in 2009. These time series present five and three simultaneous (less than half an hour) MERIS and Landsat acquisitions in 2004 and 2009, respectively, which are extremely useful for validation purposes. On the one hand, Landsat TM images were geometrically and atmospherically corrected in the preprocessing phase. It is worth nothing that only Landsat TM bands at 30 m resolution (bands 1–5 and 7) were used in this study. On the other hand, accurate MERIS geolocation information was calculated for each pixel using the AMORGOS software (ACRI-ST and ESA, 2007). Subsequently, the MERIS images were corrected atmospherically using the SCAPE-M algorithm (Guanter et al., 2008). Image time series from both sensors are atmospherically corrected to retrieve surface reflectance images in order to validate fused images and to obtain consistent biophysical temporal products (e.g. NDVI time series).

4. Experimental results

In this section, we evaluate the performance of the proposed fusion approach by using image time series from the Landsat TM and the MERIS sensors. Section 4.1 describes the quality metrics used. Section 4.2 applies our method to a test image performing a qualitative assessment in terms of visual inspection. Section 4.3 deals with the problem of tuning the free parameters of the proposed approach. Section 4.4 presents the experimental results using satellite image time series. In particular, agricultural monitoring is selected to illustrate the potential of the approach in real applications. From the analysis of the enhanced temporal profile of the NDVI during the vegetation period, including the downscaled products, a more accurate determination of the crop type and phenology can be obtained (Lunetta et al., 2010). Finally, in Section 4.5 we focus on studying the impact that co-registration, viewing geometry, and PSF effects may have on the results.

4.1. Quality assessment

The proposed image fusion method is evaluated quantitative and qualitatively. The qualitative assessment of the results is based on visual inspection by comparing the RGB and the Normalized Difference Vegetation Index (NDVI) (Tucker, 1979) of the downscaled image and the original Landsat image at the same date. The quantitative assessment is performed using several distortion metrics. Evaluation of image quality has become an active issue in image processing, mainly in denoising, coding, and image fusion applications. Currently, there is not an accepted common evaluation method to compare effectively the processed image with the reference one, thus different results can be obtained depending on the selected distortion metrics (Aiazzi et al., 2011). For this reason, several quantitative indicators are selected in this paper to compare the surface reflectance of the fused (distorted) image with the Landsat (reference) image. We firstly select standard metrics, such as root mean square error(RMSE) and Pearson's correlation coefficient (r). Then, indices more appropriated to evaluate multispectral images and fusion techniques (Alparone et al., 2007; Aiazzi et al., 2011), such as the spectral angle mapper (SAM) (Kruse et al., 1993), the Erreur Relative Globale Adimensionalle de Synthèse (ERGAS) index (Wald, 2000), and the Q4 index (Alparone et al., 2004) are also computed. The SAM index allows comparing two spectra using an angle-based error metric while the other metrics account for both radiometric and spectral errors. The ERGAS index is based on the RMSE error and is defined as:

$$\mathrm{ERGAS} = 100\frac{h}{l}\sqrt{\frac{1}{N}\sum_{i=1}^{N}\frac{\mathrm{RMSE}_i^2}{M_i^2}} \tag{8}$$

where h is the pixel size of the high spatial resolution image (Landsat TM), l is the pixel size of the low spatial resolution image (MERIS), N is the number of spectral bands used in the assessment, M_i is the mean value of the MERIS band i, and RMSE_i is the RMSE between the Landsat band i and its spectrally corresponding band from the fused image. A low ERGAS value denotes better similarity between images.

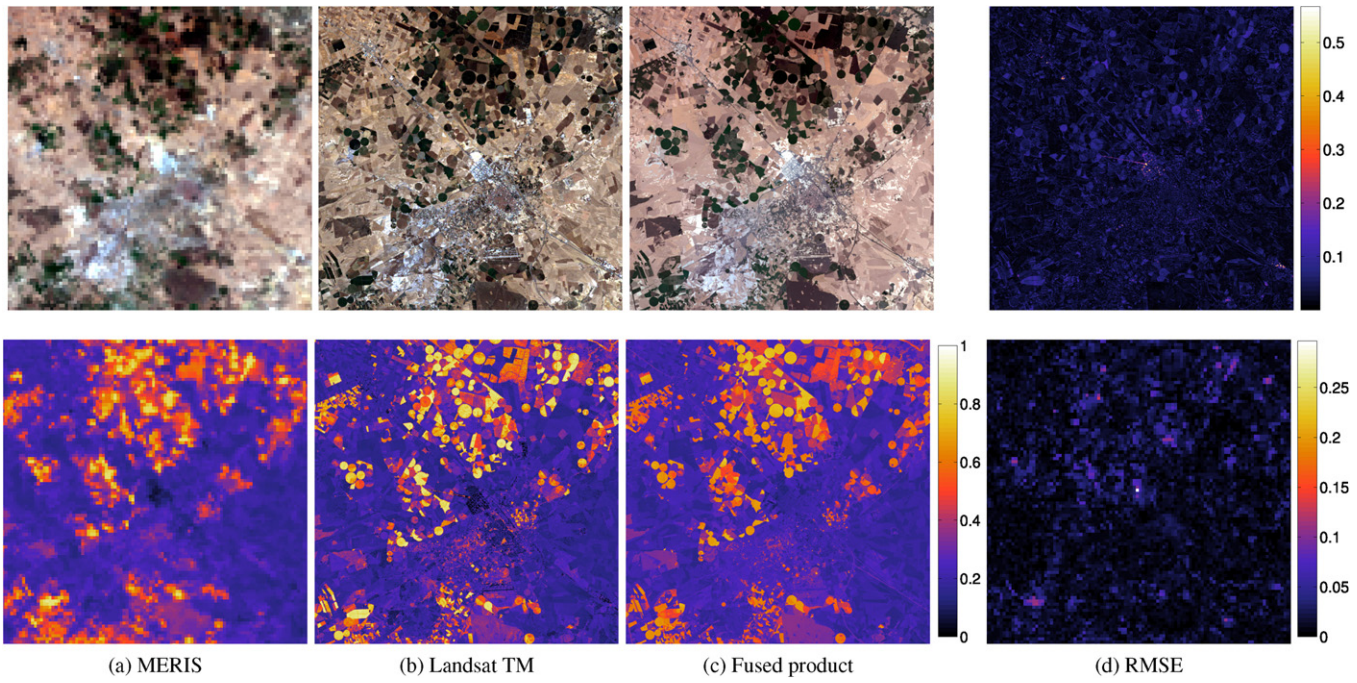

Fig. 4. RGB composition (top row) and NDVI (bottom) for the original MERIS (a) and Landsat TM (b) acquisitions, the downscaled product (c), and the RMSE values between the Landsat and the fused product at Landsat and MERIS scale (d).

The fused and the original Landsat TM images are compared in the assessment at 30 m spatial resolution. Note that the fused product provides the MERIS spectral resolution so only similar wavelengths from both instruments can be used for the assessment, i.e., bands 1–4 from the Landsat TM and 3, 5, 7, and 13 from the fused images, respectively. Additionally, we can compute the different error metrics at MERIS resolution by degrading (*upscaling*) the fused image to 300 m, taking also in this case the MERIS PSF into account. For instance, the $RMSE_M$ is computed at MERIS spatial resolution, thus accounting for the spectral distortion, while $RMSE_L$ is computed at Landsat spatial resolution and thus it better reflects the spatial distortion. Note that an additional error contribution is expected due to the different bandwidth and channel center wavelength of the sensors.

Finally, the Q4 index is a widely used similarity measure between a distorted image and a reference image having four bands in the pan-sharpening literature (Aiazzi et al., 2011). Q4 is an extension of the universal image quality index (UIQI) (Wang and Bovik, 2002), but conveniently modified using quaternions or hypercomplex numbers to account for both radiometric and spectral measurements. It is a product of three terms where the first is the correlation coefficient. The second and third terms respectively are sensitive to mean bias and contrast changes on all bands simultaneously. Q4 takes values between [0,1] and is equal to 1 only when both images are equal.

4.2. Downscaling results

In this section, we focus on the analysis of the downscaling results for the years 2004 and 2009. First, we analyze results for single MERIS acquisition. In particular, the Landsat image acquired on 01-07-2004 is used as reference and compared with the downscaled image for this date. It is worth noting that this reference image is not used by the fusion algorithm and is only used for validation purposes. The 01-07-2004 downscaled image shown in the next experiments is obtained performing the multitemporal clustering on the 24-06-2004 and 10-07-2004 Landsat images, i.e., the MERIS image was downscaled using the two closest Landsat images from the time series. All the fused images presented in this paper are obtained using the following free parameter values: number of clusters $K = 16$, spread of the clusters $m = 11$, window size $w = 11$, and regularization parameter $\alpha = 0.1$. These optimal values for the study area were selected taking into account results from a previous work (Amorós-López et al., 2011) and their impact on the results is further analyzed in Section 4.3.

In Fig. 4, the Landsat image acquired on July 1st is compared with the fused image for the RGB and the NDVI products. We can observe that both images are visually similar. The NDVI values show a Pearson's correlation coefficient of 0.87 and an average RMSE of 0.091. RMSE between the Landsat and the fused product reflectance at Landsat and MERIS spatial scales are also shown. The highest error values are located in urban areas, where the MERIS spatial resolution does not provide the required fine spatial detail or the pure pixels needed to capture the different land covers.

An additional assessment of the obtained products is carried out by analyzing the final fused spectra for different land-cover types. Fig. 5 only shows the overlapped portion of the spectrum between the fused product and the Landsat TM images. It is worth

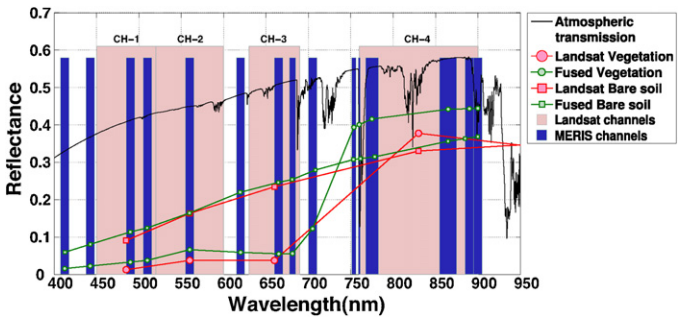

Fig. 5. MERIS and Landsat VNIR spectral channels, along with the atmospheric transmission and a vegetation and a soil spectra from the original and the fused images.

nothing that the fused spectra present 15 narrow spectral bands from MERIS in the visible and near-infrared (VNIR) range compared to the 4 wide bands of Landsat. However, the fused product does not provide information in the IR and thermal range while Landsat TM has 3 bands in this range (not shown). Fig. 5 compares vegetation and bare soil spectra in the fused image and the corresponding pixels in the Landsat image. The shapes of the spectra are well approximated with the proposed fusion approach although some underestimation is observed for the vegetation class at the 4th Landsat band. Note that the different radiometric response of the two sensors and/or the residual water vapor absorptions, which only affects Landsat/TM channel 4, may partly explain this reflectance difference in the NIR region.

4.3. Analysis of parameters

The proposed downscaling algorithm depends mainly on four parameters: number of classes (K), spread of the clusters (m), window size (w), and regularization parameter (α). The sensitivity analysis of these parameters was performed by comparing the 1st July 2004 Landsat image with the downscaled image for this date using the multitemporal setting, i.e., the example shown in the previous section. The assessment was conducted using several distortion metrics (cf. Section 4.1): RMSE, ERGAS, Pearson's correlation coefficient, spectral angle mapper (SAM), and Q4 index. From this discrepancy analysis, we selected the best parameters for this scene taking into account errors at Landsat TM and MERIS scales. For instance, in this particular analyzed image, results show the best values for $K = 16$, $m = 1.1$, $w = 11$, and $\alpha = 0.1$. This analysis was carried out following the procedure described in Amorós-López et al. (2011), where more details of the tuning of the parameters can be found. Note that for other test sites, a similar error analysis could be used to automatically determine the optimum parameters. The only requirement is to have at least one coincident Landsat and MERIS acquisition in the image time series for the test site.

4.4. Enhanced temporal profiles

Agricultural monitoring is selected as a relevant remote sensing application to demonstrate the potential of the proposed data fusion approach. An enhanced multitemporal coverage is essential for an accurate determination of the crop type and phenology. Three different fields with central pivot irrigation were selected in 2004 (Crops A–C) and two fields in 2009 (Crops D–E) to show the temporal profile of the NDVI (Fig. 6).

The NDVI evolution of the selected fields is consistent with the phenological cycles of the different vegetation types. Crop A corresponds to a summer cereal crop, whose cycle is characterized by a growth and development stages in spring followed by a drying phase. An early-spring crop that was harvested in June is shown in crop B. Note that it presents a sudden change in the temporal NDVI profile that cannot be estimated properly using only the Landsat time series. Crop C shows a double-cropped and irrigated field, in which a second crop is planted after the first one has been harvested. As noted in Crop B, a more accurate temporal NDVI profile is obtained when the downscaled MERIS images are used.

In the 2009 data set, results are similar to the previous ones. Field D corresponds to a crop whose cycle is characterized by a growth and development stages in spring followed by a drying phase. Field E shows a double-cropped irrigated field, in which a second crop is planted after the first has been harvested. As noted in the 2004 results, a more accurate temporal NDVI profile is obtained when the downscaled MERIS images are included in the time series. The main difference with the 2004 time series is that, in this case, the available MERIS images extend beyond the Landsat time series, which only cover from February to August. It is worth noting that in the last months of the year, the multitemporal clustering of Landsat images cannot be performed and thus the spatial distribution of the classes used in the downscaling is determined by the last available Landsat image in the time series. However, the obtained temporal profiles, even being less reliable in this last part of the

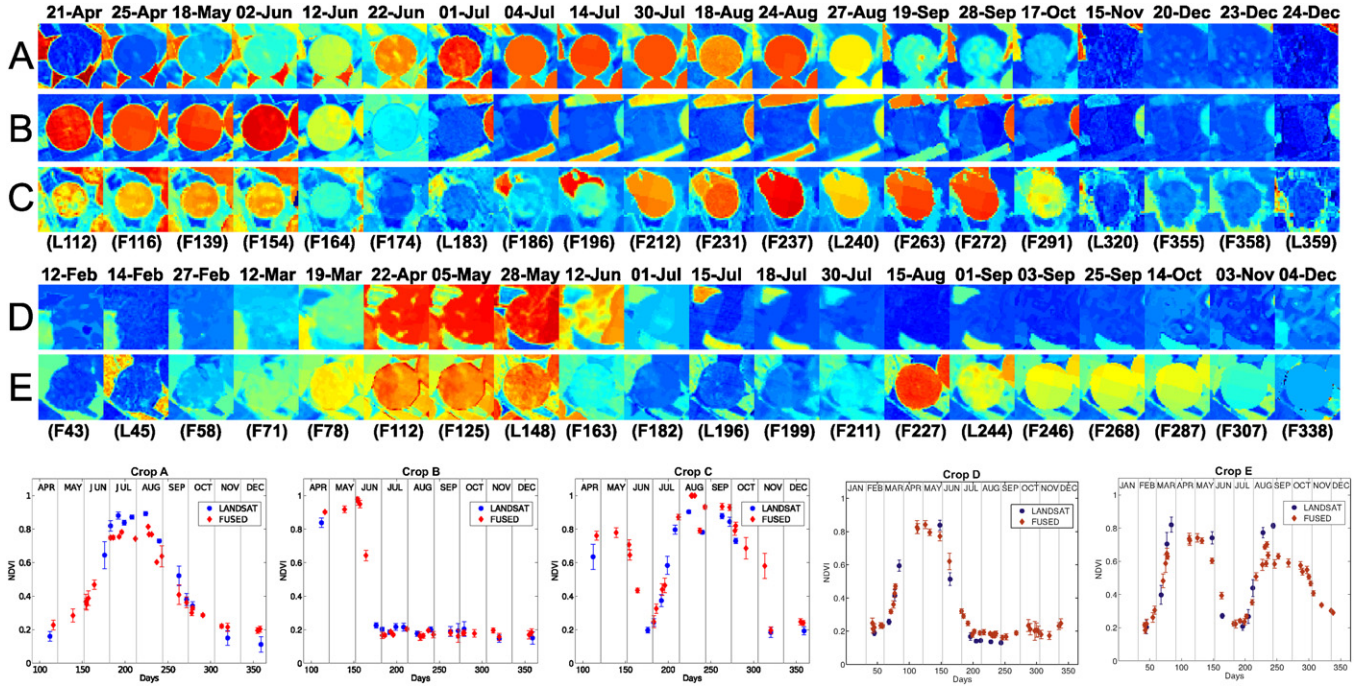

Fig. 6. Downscaling results for three (A, B and C) and two (D and E) different crop fields in 2004 and 2009, respectively. Upper panel shows the NDVI maps of the downscaled (F) and Landsat (L) images for a selected number of dates in the time series: downscaled products are noted as F followed by the day-of-year (DOY). Bottom panel shows the NDVI values (mean and standard deviations within the crop fields) derived from the Landsat-5 TM (blue dots) and the downscaled images (red diamonds). (For interpretation of references to colour in this figure legend, the reader is referred to the web version of this article.)

year, allow us to characterize the phenological cycles of the vegetation classes. In addition, these results provide information from September to December which cannot be estimated using only the available Landsat time series.

Results from both years are visually convincing, mainly due to the fact that the clustering process assigns classes that have meaningful information and possess some physical diversity, i.e., crops, urban areas, bare soil classes. This allows the algorithm to capture the spectral variability present in the scene. These good results are also related to the fact that an accurate geometric and atmospheric correction can be done in an almost flat area such as this Barrax site. Other areas might need including digital elevation models or ancillary information as well.

A quantitative assessment can also be performed by comparing the NDVI values derived from coincident dates in the time series. Fig. 7 shows the correlation (scatter plot and residuals) between the NDVI values from the five pairs of simultaneous Landsat and downscaled images in the Crop A (2004). Again, we see that good results are obtained despite of the fact that the proposed approach seems to saturate for high NDVI values (July 1st) and is not able to fully capture the NDVI variability present in the crop. This problem is mainly caused by the clustering, and occurs when a land-cover class is mainly assigned to a unique cluster, i.e., the abundance is approximately equal to one for all the pixels within the land-cover region. In this case, the same estimated class endmember in the unmixing process is assigned to the whole crop field.

Finally, we should note that a fused image is obtained not only with higher spatial resolution (30 m) but also with the MERIS spectral resolution (15 channels), see Fig. 5. This important fact can be exploited for further studies (Rast et al., 1999; Zurita-Milla et al., 2009). For instance, the MERIS spectrum could allow us to estimate accurately several biophysical parameters, such as chlorophyll content, leaf area index, fractional cover or water content, which cannot be directly estimated from Landsat TM.

4.5. Analysis of PSF impact

One of the critical issues affecting the performance of the proposed image fusion method is to ensure the correspondence between the combined high and low resolution observations. In this work, a significant effort has been done to (1) obtain an accurate pixel geolocation, (2) modify each pixel's footprint size considering the actual viewing geometry of the MERIS instrument, and (3) include the contribution of the MERIS PSF in the downscaling formulation and in the validation procedure. This section analyzes the different preprocessing steps considered for this study and their impact on the results. Different cases are considered for evaluation:

- *Case A*: MERIS pixels footprints are calculated by interpolating the pixel corners from the centers of the surrounding pixels. In this case, the pixel center coordinates are obtained from the tie points included in the MERIS FR product.
- *Case B*: MERIS pixel footprints are calculated considering the viewing geometry of the MERIS instrument. Mainly, the on-ground pixel size in the along- and across-track directions are modeled as a function of the scan angle in the field of view. Moreover, the pixels center coordinates are corrected using the AMORGOS software, which provides a more accurate geolocation.
- *Case C*: As in the previous case, pixels geolocation are also corrected with AMORGOS. In addition, abundances are calculated taking into account the PSF and the viewing geometry of the MERIS instrument.

As in the previous experiments, we illustrate the performance of the proposed algorithm by comparing the image acquired by Landsat on 01-07-2004 to the downscaled image for this date. The downscaled images for all the *A*–*C* cases are also obtained fixing the parameter values to $K = 16$, $m = 1.1$, $w = 11$, and $\alpha = 0.1$.

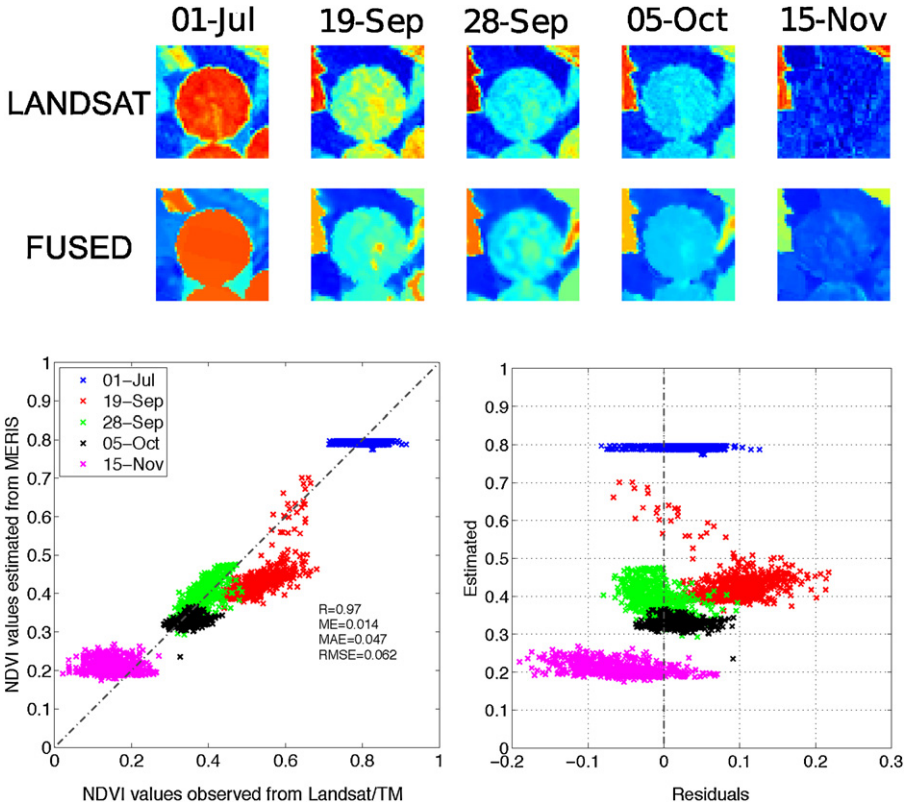

Fig. 7. Correlation analysis between the NDVI values derived from the Landsat-5 TM and the downscaled MERIS images for Crop A at the five coincident dates in 2004.

Table 1
Quality assessment using several metrics between the Landsat image and the downscaled product at Landsat and MERIS scales.

	Case	RMSE	ERGAS	CORR	SAM	Q4
Landsat scale	A	0.0471	2.4484	0.9137	5.7753	0.7296
	B	0.0395	2.0863	0.9436	4.5246	0.8493
	C	0.0390	2.0642	0.9446	4.4984	0.8581
MERIS scale	A	0.0315	1.3467	0.9638	3.0151	–
	B	0.0194	0.8026	0.9864	1.5063	–
	C	0.0192	0.7882	0.9868	1.4495	–

Table 1 shows the results for all metrics described in Section 4.1 and all the considered cases. Several conclusions can be extracted:

First, the most noticeable gain is obtained when the geolocation of the MERIS pixels is corrected using the AMORGOS software (all cases except Case *A*). This result implies that the co-registration between the images involved in the fusion must be improved as much as possible to get the best results. This effect is more evident over heterogeneous landscapes, in which few pure pixels from the MERIS image are usually found for a given land cover and co-registration inaccuracies make more difficult to locate these pure spectra since they may be erroneously calculated as mixed pixels.

Second, results improve when the acquisition geometry together with the PSF of the MERIS instrument are included (Case *C*). In this case, the PSF allows properly weighting the contribution of the different land covers within the footprint and the neighboring pixels. These results justify the proposed methodology and the improvements introduced in the preprocessing steps.

In summary, results reveal that the final fused image product can be improved by including three preprocessing steps: an accurate geolocation and co-registration, the characterization of the viewing geometry, and the PSF of the medium spatial resolution instrument.

5. Summary and conclusions

A proper exploitation of image time series is the key for studying and monitoring the Earth's environment from space. High frequency time series provide unique knowledge about the vegetation seasonal dynamics and land-cover/use changes at local and national scales. In this respect, this paper presented a multitemporal and multisensor image fusion method for combining time series of MERIS FR and Landsat TM images. The method provides images with the Landsat spatial and the MERIS spectral and temporal resolutions.

The performance of the method was illustrated in two time series acquired over Albacete, Spain, in 2004 and 2009. The temporal NDVI profiles showed that rapidly varying phenomena were captured in a more consistent way if the downscaled (fused) products are included in the time series. These temporally improved image time series allow a better support to agricultural planning by a better sampling of vegetation dynamics, such as crop monitoring, crop growth modeling and yield forecasting.

Future work is tied to determine if it is necessary to intercalibrate spectral channels from both instruments and derived products. Furthermore, results were shown for the well-known NDVI, but other indices for crop monitoring that fully exploit the MERIS spectral information can also be computed. The richer spectral information measured by MERIS allows to derive higher-level products like MERIS fAPAR (Fraction of Absorbed Photosynthetically Active Radiation) or MERIS MTCI (MERIS Terrestrial Chlorophyll Index) at an improved spatial resolution.

Finally, we would like to note that we have illustrated the performance of the algorithm in MERIS/Landsat composites, but other current and future sensors could also benefit from the proposed approach. Future GMES and contributing satellite missions like EnMAP hyperspectral or SEOSAT/INGENIO are perfect candidates to increase the temporal resolution by means of downscaled images. In particular, the instruments on board the SEOSAT/INGENIO or Sentinel-2 with Sentinel-3 systems would be a perfect fusion example of high and medium resolution instruments, respectively.

Acknowledgments

Authors want to thank the European Space Agency (ESA) and the Instituto Geográfico Nacional (IGN) for granting access to the MERIS and Landsat TM data. This paper has been supported by a IGN project, the FP7 project SenSyf 2013-2016, and the Spanish Ministry of Economy and Competitiveness (MINECO) under projects AYA2010-21432-C002-01 and TIN2012-38102-C03-01 (LIFE-VISION).

References

ACRI-ST and ESA, February 2007. The AMORGOS MERIS CFI (Accurate MERIS Ortho-Rectified Geo-location Operational Software) Software User Manual and Interface Control Document. Tech. rep., ACRI-ST and European Space Agency (Ref.: PO-ID-ACR-GS-0003).

Aiazzi, B., Alparone, L., Baronti, S., Garzelli, A., 2011. Quality assessment of pan-sharpening methods and products. IEEE Geoscience and Remote Sensing Society Newsletter 1 (161), 10–18.

Alparone, L., Baronti, S., Garzelli, A., Nencini, F., 2004. A global quality measurement of pan-sharpened multispectral imagery. IEEE Geoscience and Remote Sensing Letters 1 (October (4)), 313–317.

Alparone, L., Wald, L., Chanussot, J., Thomas, C., Gamba, P., Bruce, L., 2007. Comparison of pansharpening algorithms: outcome of the 2006 GRS-S data-fusion contest. IEEE Transactions on Geoscience and Remote Sensing 45 (October (10)), 3012–3021.

Alpaydin, E., 1998. Soft vector quantization and the EM algorithm. Neural Networks 11 (3), 457–477.

Amorós-López, J., Gómez-Chova, L., Alonso, L., Guanter, L., Moreno, J., Camps-Valls, G., 2011. Regularized multiresolution spatial unmixing for ENVISAT/MERIS and Landsat/TM image fusion. IEEE Geoscience and Remote Sensing Letters 8 (September (5)), 844–848.

Arino, O., Leroy M., Ranera F., Gross D., Bicheron P., Nino F., Defourny C.B., Vancutsem P., Achard C., Durieux F., Bourg L., Latham L., Gregorio J., Witt A.D., Herold R., Sambale M.J., Plummer S., Weber J.-L., Goryl P., Houghton N., 2007. GLOBCOVER—a global land cover service with MERIS. In: Proceedings ESA Living Planet Symposium, held in Montreux, Switzerland, pp. 1–6.

Camps-Valls, G., Tuia, D., Gómez-Chova, L., Jiménez, S., Malo, J., 2011. Remote Sensing Image Processing. Morgan & Claypool, LaPorte, CO, USA.

Carrão, H., Araújo, A., Gonçalves, P., Caetano, M., 2010. Multitemporal MERIS images for land-cover mapping at a national scale: a case study of Portugal. International Journal of Remote Sensing 31 (8), 2063–2082.

Clevers, J., Schaepman, M., Mücher, C., de Wit, A., Zurita-Milla, R., Bartholomeus, H., 2007. Using MERIS on Envisat for land cover mapping in the Netherlands. International Journal of Remote Sensing 28 (January (3–4)), 637–652.

Dash, J., Mathur, A., Foody, G.M., Curran, P.J., Chipman, J.W., Lillesand, T.M., 2007. Land cover classification using multi-temporal meris vegetation indices. International Journal of Remote Sensing 28 (6), 1137–1159.

Gao, F., Masek, J., Schwaller, M., Hall, F., 2006. On the blending of the Landsat and MODIS surface reflectance: predicting daily Landsat surface reflectance. IEEE Transactions on Geoscience and Remote Sensing 44 (August (8)), 2207–2218.

Gómez-Chova, L., Zurita-Milla, R., Alonso, L., Amorós-López, J., Guanter, L., Camps-Valls, G., 2011. Gridding artifacts on medium-resolution satellite image time series: MERIS case study. IEEE Transactions on Geoscience and Remote Sensing 49 (July (7)), 2601–2611.

Goshtasby, A., Nikolov, S., 2007. Image fusion: Advances in the state of the art. Information Fusion 8 (2), 114–118.

Guanter, L., Gómez-Chova, L., Moreno, J., 2008. Coupled retrieval of aerosol optical thickness, columnar water vapor and surface reflectance maps from ENVISAT/MERIS data over land. Remote Sensing of Environment 112 (June (6)), 2898–2913.

Hall, D., Llinas, J., 1997. An introduction to multisensor data fusion. Proceedings of the IEEE 85 (January (1)), 6–23.
Keshava, N., Mustard, J., 2002. Spectral Unmixing. IEEE Signal Processing Magazine 19 (January (1)), 44–57.
Khan, M., Alparone, L., Chanussot, J., 2009. Pansharpening quality assessment using the modulation transfer functions of instruments. IEEE Transactions on Geoscience and Remote Sensing 47 (November (11)), 3880–3891.
Kohonen, T., 2001. Self-Organizing Maps, vol. 30., 3rd ed. Springer Series in Information Sciences.
Kruse, F., Lefkoff, A., Boardman, J., Heidebrecht, K., Shapiro, A., Barloon, P., Goetz, A., 1993. The spectral image processing system (SIPS)-interactive visualization and analysis of imaging spectrometer data. Remote Sensing of Environment 44 (2–3), 145–163.
Lunetta, R.S., Shao, Y., Ediriwickrema, J., Lyon, J.G., 2010. Monitoring agricultural cropping patterns across the Laurentian Great Lakes Basin using MODIS-NDVI data. International Journal of Applied Earth Observation and Geoinformation 12 (2), 81–88.
Minghelli-Roman, A., Mangolini, M., Petit, M., Polidori, L., 2001. Spatial resolution improvement of MERIS images by fusion with TM images. IEEE Transactions on Geoscience and Remote Sensing 39 (July (7)), 1533–1536.
Minghelli-Roman, A., Polidori, L., Mathieu-Blanc, S., Loubersac, L., Cauneau, F., 2006. Spatial resolution improvement by merging MERIS-ETM images for coastal water monitoring. IEEE Geoscience and Remote Sensing Letters 3 (April (2)), 227–231.
Park, J., Nab, S., 2007. MODIS and Landsat TM data image fusion based on improved resolution method: assessing the quality of resulting NDVI images. In: Neale, C.M.U., Owe, M., D'Urso, G. (Eds.), Proceedings of SPIE: Remote Sensing for Agriculture, Ecosystems, and Hydrology IX, vol. 6742. 18–20 September, Florence, Italy, pp. 67420S.1–10.
Pellemans, A., Jordans, R., Allewijn, R., 1993. Merging multispectral and panchromatic SPOT images with respect to the radiometric properties of the sensor. Photogrammetric Engineering & Remote Sensing 59 (1), 81–87.
Plaza, A., Martínez, P., Pérez, R., Plaza, J., 2004. A quantitative and comparative analysis of endmember extraction algorithms from hyperspectral data. IEEE Transactions on Geoscience and Remote Sensing 42 (March (3)), 650–663.
Plaza, J., Hendrix, E., García, I., Martín, G., Plaza, A., 2011. On endmember identification in hyperspectral images without pure pixels: a comparison of algorithms. Journal of Mathematical Imaging and Vision, 1–13.
Pohl, C., Van Genderen, J., 1998. Multisensor image fusion in remote sensing: concepts, methods and applications. International Journal of Remote Sensing 19 (March (5)), 823–854.
Rast, M., Bézy, J., Bruzzi, S., 1999. The ESA medium resolution imaging spectrometer MERIS: a review of the instrument and its mission. International Journal of Remote Sensing 20 (June (9)), 1681–1702.
Stathaki, T., 2008. Image Fusion: Algorithms and Applications. Academic Press.
Thomas, C., Ranchin, T., Wald, L., Chanussot, J., 2008. Synthesis of multispectral images to high spatial resolution: a critical review of fusion methods based on remote sensing physics. IEEE Transactions on Geoscience and Remote Sensing 46 (May (5)), 1301–1312.
Tucker, C., 1979. Red and photographic infrared linear combinations for monitoring vegetation. Remote Sensing of Environment 8 (2), 127–150.
Van der Meer, F.D., Jia, X., 2012. Collinearity and orthogonality of endmembers in linear spectral unmixing. International Journal of Applied Earth Observation and Geoinformation 18 (0), 491–503.
Wald, L., 2000. Quality of high resolution synthesized images: Is there a simple criterion? In: Ranchin, T., Wald, L. (Eds.), Int. Conf. on Fusion of Earth Data. , pp. 99–103.
Wang, Z., Bovik, A., 2002. A universal image quality index. IEEE Signal Processing Letters 9 (March (3)), 81–84.
Wang, Z., Ziou, D., Armenakis, C., Li, D., Li, Q., 2005. A comparative analysis of image fusion methods. IEEE Transactions on Geoscience and Remote Sensing 43 (June (6)), 1391–1402.
Zhang, Y., 2004. Understanding image fusion. Photogrammetric Engineering & Remote Sensing 70 (June), 657–661.
Zhukov, B., Oertel, D., Lanzl, F., Reinhackel, G., 1999. Unmixing-based multisensor multiresolution image fusion. IEEE Transactions on Geoscience and Remote Sensing 37 (May (3)), 1212–1226.
Zurita-Milla, R., Clevers, J., Schaepman, M., 2008. Unmixing-based Landsat TM and MERIS FR data fusion. IEEE Geoscience and Remote Sensing Letters 5 (July (3)), 453–457.
Zurita-Milla, R., Clevers, J., Van Gijsel, J., Schaepman, M., 2011. Using MERIS fused images for land-cover mapping and vegetation status assessment in heterogeneous landscapes. International Journal of Remote Sensing 32 (4), 973–991.
Zurita-Milla, R., Kaiser, G., Clevers, J., Schneider, W., Schaepman, M., 2009. Downscaling time series of MERIS full resolution data to monitor vegetation seasonal dynamics. Remote Sensing of Environment 113 (September (9)), 1874–1885.